HHS Public Access

Author manuscript

Nat Commun. Author manuscript; available in PMC 2015 January 11.

Published in final edited form as:

Nat Commun. ; 5: 4350. doi:10.1038/ncomms5350.

A distinct sodium channel voltage-sensor locus determines insect selectivity of the spider toxin Dc1a

Niraj S Bende[1], **Slawomir Dziemborowicz**[2], **Mehdi Mobli**[3], **Volker Herzig**[1], **John Gilchrist**[4], **Jordan Wagner**[4], **Graham M Nicholson**[2], **Glenn F King**[1,*], and **Frank Bosmans**[4,5,*]

[1]Institute for Molecular Bioscience, The University of Queensland, St. Lucia, QLD 4072 Australia

[2]School of Medical & Molecular Biosciences, University of Technology, Sydney, Broadway, NSW 2007 Australia

[3]Centre for Advanced Imaging, The University of Queensland, St. Lucia, QLD 4072 Australia

[4]Department of Physiology, Johns Hopkins University, School of Medicine, Baltimore, MD 21205 USA

[5]Solomon H. Snyder Department of Neuroscience, Johns Hopkins University, School of Medicine, Baltimore, MD 21205 USA

Abstract

β-Diguetoxin-Dc1a (Dc1a) is a toxin from the desert bush spider *Diguetia canities* that incapacitates insects at concentrations that are non-toxic to mammals. Dc1a promotes opening of German cockroach voltage-gated sodium (Na_v) channels ($BgNa_v1$), whereas human Na_v channels are insensitive. Here, by transplanting commonly targeted S3b-S4 paddle motifs within $BgNa_v1$ voltage sensors into $K_v2.1$, we find that Dc1a interacts with the domain II voltage sensor. In contrast, Dc1a has little effect on sodium currents mediated by $PaNa_v1$ channels from the American cockroach even though their domain II paddle motifs are identical. When exploring regions responsible for $PaNa_v1$ resistance to Dc1a, we identified two residues within the $BgNa_v1$ domain II S1–S2 loop that when mutated to their $PaNa_v1$ counterparts drastically reduce toxin susceptibility. Overall, our results reveal a distinct region within insect Na_v channels that helps determine Dc1a sensitivity, aconcept that will be valuable for the design of insect-selective insecticides.

*Address correspondence to Glenn F King (glenn.king@imb.uq.edu.au) or Frank Bosmans (frankbosmans@jhmi.edu).

Author contributions

N.S.B, S.D., M.M., V.H., J.G., G.M.N., G.F.K, and F.B. designed research, N.S.B, S.D., M.M., V.H., J.G., J.W., G.M.N., G.F.K, and F.B. performed research; N.S.B, S.D., M.M., V.H., G.M.N., G.F.K, and F.B. analyzed data; N.S.B, S.D., M.M., V.H., G.M.N., G.F.K, and F.B wrote the paper.

Competing financial interests: The authors declare no competing financial interests.

Accession codes: Complete chemical shift assignments for rDc1a have been deposited in BioMagResBank under accession code 19666.

Keywords

voltage-gated sodium channel; voltage sensor; spider toxin; Dc1a; insect; cockroach

Introduction

Insect voltage-gated sodium (Na_v) channels share a common architecture with their mammalian orthologues[1]. The pore-forming subunit consists of four connected domains (DI-IV), each with six transmembrane segments (S1–S6). These homologous but not identical domains each contain a voltage sensor (S1–S4) and a portion of the pore through which Na^+ can diffuse (S5–S6)[2]. While they have yet to be identified in insect Na_v channels, each voltage-sensing domain within mammalian and bacterial Na_v channels contains an S3b-S4 helix-turn-helix motif, the voltage-sensor paddle, which drives voltage-sensor activation[3, 4, 5, 6]. Aside from its vital role in channel gating, the paddle motif is also an important pharmacological target, as peptide toxins interact with this region to modify channel opening[3, 4, 7]. Insect Na_v channels likely possess similar motifs since residue substitutions in homologous regions can abolish channel susceptibility to toxins found in animal venoms[1]. Even though voltage-sensing domains are extensively targeted by naturally occurring peptides, commercially available insecticides such as pyrethroids and oxadiazines typically interact with the channel pore region or intracellular linker between S4 and S5 to disrupt opening or closing (*i.e.* gating)[8, 9]. However, insects have responded to this threat by mutating residues at strategic locations within the channel that result in a reduced sensitivity to these compounds[9]. Moreover, the conserved nature of the Na_v channel pore throughout the animal kingdom often leads to undesired biological activity of insecticides in beneficial insect orders or mammals[8, 9, 10]. Since the amino acid composition of voltage-sensing domains varies considerably between related Na_v-channel isoforms, these regions may replace the pore as a target for designing insecticides with a higher degree of phyletic selectivity, an intriguing notion that has yet to be fully explored.

Na_v channels have been governing electrical excitability in a wide range of organisms for millions of years, even before the development of neurons[2, 11]. Thus, it is not surprising that ancient organisms such as spiders developed an arsenal of toxins geared towards incapacitating prey by modulating Na_v channel function[12, 13, 14, 15]. One intriguing specimen is the desert bush spider (*Diguetia canities*) whose habitat spans the Southwestern deserts of the United States[16, 17]. The venom of this relatively unexplored primitive weaving spider contains a 57-residue peptide known as DTX9.2 (or β-diguetoxin-Dc1a[18], hereafter Dc1a) (Fig. 1a), one of the most potent insect-selective neurotoxins found in arthropod venoms[19]. Although its precise molecular target has yet to be elucidated, neurophysiological studies on housefly larvae revealed excitation of sensory and neuromuscular preparations upon Dc1a application that could be blocked by the Na_v channel-blocking compound tetrodotoxin (TTX)[20].

Here, we show that Dc1a potently promotes opening of the German cockroach Na_v channel $BgNa_v1$[21] by interacting with the paddle motif in domain II. Surprisingly, Dc1a has little effect on $PaNa_v1$-expressing neurons isolated from the American cockroach (*Periplaneta*

americana)[22], even though the toxin binding site is identical in these two cockroach channels. By exploring regions responsible for the remarkable insect-family specificity of Dc1a, we uncovered an important role for the domain II S1–S2 loop in determining $PaNa_v1$ resistance to Dc1a. Together with the unique solution structure of Dc1a, our results provide a proof of concept that toxins – and by extension small molecules – can selectively target insect Na_v channels by interacting with their voltage-sensing domains, thus facilitating the development of new insecticides.

Results

Production of recombinant Dc1a

We first produced recombinant Dc1a peptide (rDc1a) using a novel approach that addresses the challenge of correctly folding disulfide-rich spider toxins in *E. coli*[23]. To this end, we created an IPTG-inducible construct (Fig. 1b) that allows for export of a His_6-MBP-Dc1a fusion protein to the *E. coli* periplasm, where the enzymes involved in disulfide-bond formation are located[23]. Upon recovery from the soluble cell fraction, the fusion protein was purified using nickel affinity chromatography (Fig. 1c). Subsequent cleavage and chromatographic purification yielded a single major disulfide-bond isomer with a purity of >98% as assessed by SDS-PAGE and MALDI-TOF mass spectrometry (Fig. 1d). (Note that, with four disulfide bonds, there are 105 possible disulfide-bond isomers of rDc1a.) Overall, the final yield was ~1.1 mg of toxin per litre of culture. Since native Dc1a was unavailable to us, we confirmed the insecticidal activity of rDc1a by injection into the blowfly *Lucilia cuprina* and the housefly *Musca domestica*, which yielded LD_{50} values of 231 ± 32 pmol/g and 493 ± 52 pmol/g, respectively (n = 3) (Supplementary Fig. 1). We therefore conclude that rDc1a has a similar lethality to agricultural pests when compared to native toxin[19].

Solution structure of rDc1a

The development of an efficient bacterial expression system allowed us to produce uniformly $^{13}C/^{15}N$-labelled rDc1a protein for structure determination using heteronuclear NMR. ^1H_N, ^{15}N, $^{13}C_\alpha$, $^{13}C_\beta$, and $^{13}C'$ resonance assignments for the toxin were obtained from analysis of amide-proton strips in 3D HNCACB, CBCA(CO)NH, and HNCO spectra. Sidechain ^1H and ^{13}C chemical shifts were obtained using a 4D HCC(CO)NH-TOCSY experiment, which has the advantage of providing sidechain ^1H-^{13}C connectivities[24]. Complete chemical shift assignments have been deposited in BioMagResBank (Accession Number 19666). CYANA was used for automated NOESY assignment and structure calculation[25]. The disulfide-bond pattern (1–4, 2–5, 3–8, 6–7) was unambiguously determined from preliminary structures calculated without disulfide-bond restraints[26] and is identical to the framework predicted in the UniProtKB entry for Dc1a (P49126). Of the 200 structures that were calculated from random starting conformations, 20 conformers with high stereochemical quality (as judged by MolProbity[27]) were selected to represent the solution structure of rDc1a (Fig. 2a). Atomic coordinates for the final ensemble of 20 structures are available from the Protein Data Bank (PDB; Accession Number 2MI5).

Statistics highlighting the high precision and stereochemical quality of the ensemble of rDc1a structures are shown in Supplementary Table 1. The average MolProbity score of

1.24 places the ensemble in the 99th percentile relative to all other structures ranked by MolProbity. The high stereochemical quality of the ensemble stems from a complete absence of bad close contacts and an excellent Ramachandran plot quality (>99% of residues in the most favoured region). The structural ensemble is also highly precise with backbone and heavy-atom RMSD values over all the structural ordered regions (residues 3–42, 52–56) of 0.27 ± 0.07 Å and 0.70 ± 0.11 Å, respectively. The ensemble of rDc1a structures ranks as "very high resolution" based on these measures of precision and stereochemical quality[28].

Three of the four disulfide bonds in rDc1a form a classical inhibitor cysteine knot (ICK) motif in which the Cys13–Cys26 and Cys20–Cys40 disulfide bonds and the intervening sections of the polypeptide backbone forming a 23-residue ring that is pierced by the Cys25–Cys54 disulfide bond (Fig. 2b). This ICK motif is commonly found in spider toxins, and this particular scaffold provides these peptides (so-called knottins) with an unusually high degree of chemical, thermal and biological stability[15]. However, the structure of rDc1a differs markedly from other ICK toxins, and a DALI search[29] of the PDB returned no structural homologs. First, rDc1a contains an additional disulfide bond (Cys42–Cys52) that appears to serve as a molecular staple which limits the flexibility of a disordered serine-rich hairpin loop (residues 43–51) (Fig. 2b). Stapled hairpins of this kind have been observed in only a small number of spider toxins[30]. Second, the extended N-terminus of rDc1a along with an unusually large loop between Cys26 and Cys40 enables the formation of an N-terminal three-stranded antiparallel β-sheet that is not found in any other knottin (Fig. 2b,c). The uniqueness of the rDc1a structure can readily be seen by comparison with the structure of As1a, a typical spider-venom-derived knottin that modulates the activity of insect Na_V channels[30]. The two toxins can be aligned over their core ICK regions with an rmsd of 1.9 Å (Fig. 2c) consistent with them both being members of the knottin family. However, when aligned over this ICK region, the N-terminal β-sheet of rDc1a is entirely separate to the region of structural overlap (Fig. 2c). Despite its structural uniqueness, the molecular surface of rDc1a contains a relatively uniform distribution of charged residues (Fig. 2d); moreover, there are no distinct clusters of hydrophobic residues that might mediate an interaction with lipid bilayers[7, 31] (Supplementary Movie 1).

rDc1a opens the German cockroach Na_V channel $BgNa_V1$

Diguetia spiders are generalist predators and their diet consists of various insects ranging from small ants to sizeable prey such as grasshoppers and cockroaches[16, 32]. As such, we decided to test whether rDc1a influences the gating properties of $BgNa_v1$, a well-studied Na_v channel isoform cloned from the German cockroach[8, 21]. We functionally expressed $BgNa_v1$ in *Xenopus* oocytes and applied various concentrations of rDc1a. At 1 μM, rDc1a produced robust opening of $BgNa_v1$ at voltages where the channel is normally closed. This was achieved by drastically shifting channel activation to more negative potentials [$V_{1/2}$ was shifted from −27.3 ± 0.2 mV (mean ± standard error of the mean – SEM) (slope 4.0 ± 0.2) to −49.4 ± 0.4 mV (slope 3.5 ± 0.3) in the presence of 1 μM rDc1a; Fig. 3a] whereas steady-state inactivation (or channel availability) was only slightly affected ($V_{1/2}$ was shifted from −52.2 ± 0.1 mV to −55.1 ± 0.1 mV in the presence of 1 μM rDc1a; Fig. 3a). The rate of recovery from fast inactivation was also not significantly altered (τ is 2.1 ± 0.1 ms *vs.* 2.2 ± 0.1 ms) (Fig. 3b). Upon addition of 1 μM rDc1a to channels depolarized to −60 mV every 5

s, sodium currents became rapidly visible as a result of the −22 mV shift in voltage-dependent opening of $BgNa_v1$ (Fig. 3c). Moreover, rDc1a similarly affects the channel when voltage-steps to −60mV were applied every 50 s, suggesting that the toxin can access its binding site when $BgNa_v1$ is in the resting state[12]. Channels completely recovered following washout in toxin-free solution (Fig. 3c). The persistent nature of the emerging current does not stem from the inhibition of fast inactivation by rDc1a since wild-type (WT) $BgNa_v1$ inherently possesses these characteristics at mildly depolarizing voltages[33]. Fitting the Hill equation to the concentration dependence for toxin-induced current potentiation, as determined by shifts in $V_{1/2}$, yielded an EC_{50} of 65 ± 1 nM and a Hill coefficient of 1.19 ± 0.02 (Fig. 3d), suggesting that the toxin may interact with only one binding site.

Interestingly, 1 μM rDc1a did not affect any of the tested vertebrate Na_v channel isoforms or the hERG channel[34], a member of the cardiac voltage-gated potassium (K_v) channel family and an FDA-mandated screening target for potential off-target drug effects (Supplementary Fig. 2a). These results are consistent with the report that Dc1a has no effect in mice when injected intraperitoneally or intracerebroventricularly at doses of 4.1 and 1.0 mg/kg, respectively[19].

rDc1a interacts with the domain II paddle motif in $BgNa_v1$

Subsequently, we were interested in identifying the receptor sites for rDc1a within insect Na_v channels that result in such a profound shift in the voltage-dependence of activation. Our experiments with $BgNa_v1$ suggest that rDc1a functions as an excitatory toxin to activate insect Na_v channels at membrane voltages where they are normally closed. Hence, the toxin may interact with S3b-S4 paddle motifs within $BgNa_v1$ voltage sensors in a manner analogous to previously described β-scorpion toxins[3, 35, 36]. In order to test this hypothesis, we first needed to establish whether $BgNa_v1$ contains paddle motifs with similar functions as in K_v channels[37, 38, 39] and in mammalian Na_v channel isoforms where they have been identified ($rNa_v1.2a$, $rNa_v1.4$, $rNa_v1.8$, $rNa_v1.9$, and $hNa_v1.9$)[3, 4]. To this end, we employed a previously reported approach in which specific S3b-S4 regions from each voltage-sensing domain of a Na_v channel were transplanted into homotetrameric K_v channels (Fig. 4a)[3, 4, 7]. After several attempts (Fig. 4a), we were able to generate functional chimeras between $BgNa_v1$ and $K_v2.1$ using known paddle motif boundaries[3, 4] (Fig. 4a–b). All of the constructs contain the crucial basic residues that contribute to gating charge movement in K_v channels[40, 41], suggesting that each of the four voltage-sensing domains in $BgNa_v1$ contain paddle motifs that are capable of sensing membrane voltage changes.

Examination of the conductance-voltage (*G-V*) relationships for the $BgNa_v1/K_v2.1$ chimeras reveals that each of the four voltage-sensor paddles has a distinct effect on the gating properties of $K_v2.1$. This was evidenced by marked differences in the midpoints of activation for the *G-V* relations for the domain I, II, and IV constructs which are ≥50 mV, 13 ± 2 mV, and −9 ± 2 mV, respectively (Fig. 4c). The *G-V* relationship for the domain III $BgNa_v1/K_v2.1$ construct is bimodal, suggesting that the functional coupling between the voltage-sensing domains and the pore has been considerably altered. Although the underlying mechanism is unclear, it is possible that pore opening in this particular chimera may occur when: *1)* not all four voltage sensors are fully activated[42]; or *2)* each voltage

sensor has transferred only a portion of its charge across the hydrophobic septum[43, 44, 45]. The latter scenario seems more likely since in the related *Shaker* K_v channel, all four voltage sensor need to be in the active position before the pore opens[42, 46]. Moreover, intermediate states have also been observed when measuring gating currents of the *Shaker* K_v channel in which a mutation immobilized voltage-sensor movement between the resting and activated states, thereby shifting the voltage activation of the ionic currents[47]. Finally, it is worth mentioning that the domain III $BgNa_v1/K_v2.1$ construct may display multiple open states according to a model that has been described for N-type Ca_v channels[48].

Remarkably, domain IV paddle motifs from $rNa_v1.2a$ and $rNa_v1.4$ slow activation kinetics when transplanted into K_v channels. These observations support the notion that the domain IV paddle motif contributes substantially to the overall rate of voltage-sensor activation[3, 4]. To explore whether the domain IV paddle motif serves a similar role in $BgNa_v1$, we measured the kinetics of activation and deactivation of the four $BgNa_v1$ paddle constructs in response to membrane depolarization and repolarization, respectively. Similar to previously studied chimeric channels, the activation and deactivation kinetics observed for the domain IV construct of $BgNa_v1/K_v2.1$ are slower over a wide voltage range when compared to the other domains (Fig. 4d), suggesting that this particular domain may indeed contribute to fast inactivation in insect Na_v channels[49, 50, 51]. We obtained additional evidence for the functional role of the domain IV paddle motif in $BgNa_v1$ gating from experiments with BomIV, a classic insect-selective α-scorpion toxin from the venom of *Buthus occitanus mardochei* that inhibits fast inactivation in American cockroach neurons[52]. To determine whether BomIV influences $BgNa_v1$ in a similar fashion, we applied 10 nM to channel-expressing *Xenopus* oocytes and observed that the toxin indeed slows down fast inactivation (Supplementary Fig. 2b). Subsequent testing on the $BgNa_v1/K_v2.1$ chimeras revealed that BomIV does not affect WT $K_v2.1$ or the domain I, II, and III constructs. However, a dramatic toxin-induced inhibition of the domain IV chimera corroborates the importance of this particular voltage-sensing domain in toxin binding and $BgNa_v1$ fast inactivation (Supplementary Fig. 2b).

We next investigated whether rDc1a modulates the activity of any of the four $BgNa_v1/K_v2.1$ paddle chimeras and found that 1 μM rDc1a exclusively interacts with the domain II construct whereas domains I, III, IV, and WT $K_v2.1$ are unaffected (Fig. 4e, Supplementary Fig. 2c). This result suggests that rDc1a specifically targets the domain II voltage sensor within $BgNa_v1$ to influence channel opening.

rDc1a distinguishes between cockroach Na_v1 channels

Since the domain II paddle motif in $BgNa_v1$[21] is identical to that in $PaNa_v1$[22], we expected a similar effect of rDc1a in whole-cell patch-clamp recordings from American cockroach dorsal unpaired median (DUM) neurons. Surprisingly, 1 μM rDc1a had little effect on sodium current amplitude or kinetics in DUM neurons as reflected in the threshold, or $V_{1/2}$, of Na_v channel activation or the $V_{1/2}$ of steady-state inactivation measurements (Supplementary Fig. 3). Furthermore, there were no significant use-dependent effects on sodium current amplitude or kinetics.

Due to the unexpectedly weak effects of 1 μM rDc1a on voltage-dependent activation of *P. americana* DUM neurons compared to $BgNa_v1$ channels from *B. germanica*, acute toxicity assays were expanded to include both cockroach species (Fig. 5a,b). Remarkably, these bioassays revealed lethal toxicity of rDc1a in *B. germanica* compared to only mild, reversible effects in *P. americana*. At doses up to 5 nmol/g, rDc1a generated only minor spastic contractions of the abdomen, some shaking, and evidence of reduced motor activity in *P. americana*. Even though these effects were completely reversible, a very small percentage of cockroaches did develop paralysis after 24 h (7 ± 7% knockdown, $n = 3$). One explanation for these observations may be toxin binding to a subset of Na_v channel splice variants[53] or the presence of endogenous pharmacologically active auxiliary subunits[54]. Conversely, *B. germanica* underwent dose-dependent flaccid or contractile paralysis, and lethality was observed after 8 h at all doses tested (Fig. 5a). The KD_{50} and LD_{50} values at 24 h post injection were 3.0 ± 1.2 nmol/g and 4.2 ± 3.4 nmol/g ($n = 3$), respectively. These observations suggest that residues in regions outside of the domain II paddle motif may underlie the remarkably different sensitivity of $BgNa_v1$ and $PaNa_v1$ to rDc1a.

The S1–S2 loop modulates Na_v channel sensitivity to rDc1a

Sequence alignment of $BgNa_v1$ with $PaNa_v1$ reveals a highly conserved S1–S4 voltage sensor in domain II with only three amino acid substitutions (Fig. 6a; Supplementary Fig. 4). Of those, two residues in the S1–S2 loop are potentially accessible for a peptide toxin applied from the extracellular environment (His805 and Asp812 in $BgNa_v1$ which correspond to a Tyr and Glu in $PaNa_v1$, respectively). Upon mutating these residues in $BgNa_v1$ to their $PaNa_v1$ counterparts, the resulting $BgNa_v1^{YE}$ construct functionally expressed in *Xenopus* oocytes with a voltage-dependent activation $V_{1/2}$ of −41.5 ± 0.3 mV and a steady-state inactivation $V_{1/2}$ of −56.4 ± 0.2 mV (Fig. 6b). Unfortunately, a functional $PaNa_v1$ clone was unavailable to undertake gain-of-function experiments. Strikingly, 100 nM rDc1a was no longer sufficient to open $BgNa_v1^{YE}$ whereas this concentration generated large inward sodium currents when applied to WT channels (Fig. 6c, inset). When surveying higher concentrations of rDc1a, it becomes clear that concentrations of more than 1 μM are required to achieve a potentiation with $BgNa_v1^{YE}$ that is comparable to the WT channel (EC_{50} ~65 nM) (Fig. 6c). Although we cannot exclude the possibility that rDc1a interacts with other $PaNa_v1$ domains at such concentrations, administering high doses of the toxin is indeed mildly toxic to *P. americana* (Fig. 5a,b). Thus, our mutagenesis experiments have uncovered a novel region within insect Na_v channels that helps determine their sensitivity to spider toxins. This locus contributes to the drastically reduced sensitivity of the American cockroach to rDc1a from the venom of the desert bush spider whereas its German counterpart is highly susceptible.

Discussion

The initial goal of this study was to explore the mechanism underlying the efficacy of Dc1a, a potent insecticidal peptide toxin produced by desert bush spiders. To this end, we first produced recombinant rDc1a and determined its solution structure using heteronuclear NMR (Fig. 1 and 2). Next, we tested rDc1a on the heterologously expressed German cockroach channel $BgNa_v1$ and discovered that the toxin dramatically promotes channel opening (Fig.

3). By taking advantage of the portable nature of S3b–S4 paddle motifs within voltage-sensing domains[3, 4, 7, 38], we demonstrated that such motifs also exist in each of the four voltage-sensing domains of $BgNa_v1$, and that rDc1a selectively interacts with the paddle motif in domain II, a feature that it shares with an extensive list of animal toxins that target this particular paddle motif[3, 4, 12, 55, 56], albeit with a high degree of insect selectivity (Fig. 4). Remarkably, our insect assays revealed that German cockroaches are highly susceptible to rDc1a whereas the closely related American cockroach is virtually insensitive despite the fact that the domain II paddle motif in $BgNa_v1$ is identical to that in $PaNa_v1$ (Fig. 5 and Supplementary Fig. 4). To elucidate the machinery responsible for this discrepancy, we mutated two residues in the S1–S2 loop that differ between $BgNa_v1$ and $PaNa_v1$ (His805 and Asp812) and found that the susceptibility of the resulting $BgNa_v1^{YE}$ construct to rDc1a is dramatically reduced (Fig. 6). Interestingly, mammalian Na_v channel isoforms possess a Tyr and Ser at the corresponding positions, which presumably contributes to their insensitivity to rDc1a; however, their domain II paddle motif differs as well (Supplementary Fig. 4).

It is interesting to consider potential mechanisms that may underlie the insect-family specificity of rDc1a. For example, the β3–β4 hairpin (Fig. 2b) often houses the pharmacophore in spider ICK toxins that target voltage-gated ion channels[57], but the unusual architecture of rDc1a (Fig. 2c) and its unique ability to dramatically promote opening of insect Na_v channels (Fig. 3) suggests that it might interact with the voltage sensors of these channels in a unique manner. As such, the domain II S1–S2 loop may play a role in positioning the toxin into a water-filled cavity adjacent to the S3–S4 paddle motif[58], thereby placing particular toxin residues in strategic positions to stabilize the domain II voltage sensor in an activated position. This hypothesis is strengthened by the observation that the substitution of two residues in the domain II S1–S2 loop within mammalian $Na_v1.2$ channels decreases sensitivity to the functionally related β-scorpion toxin CssIV by a factor of four[59]. Another possible mechanism is that rDc1a binding to the domain II S1–S2 loop in $BgNa_v1$ allosterically influences channel opening. Such a hypothesis was postulated when a domain III S1 splice variant of $BgNa_v1$ revealed an increased susceptibility to the insect-selective β-scorpion toxin Lqh-dprIT$_3$[60]. However, one caveat is that a depolarizing prepulse is needed to potentiate the maximal effect of CssIV and Lqh-dprIT$_3$[49,50]. Similar to the structurally unrelated spider toxin Magi5 which activates rat $Na_v1.2$ channels by binding to the domain II voltage sensor[61], rDc1a does not require such a prepulse.

In summary, the current study provides a molecular explanation for the remarkable insect selectivity of Dc1a, the most potent insecticidal toxin identified in the venom of the desert bush spider. Moreover, we have uncovered a novel toxin receptor site within insect Na_v channels that provides a new framework for the design of molecules capable of targeting specific insect families. This knowledge may be used in the future to develop insecticides that target specific insect pests without affecting beneficial insects or endangering human health.

Methods

Chemicals

All chemicals were purchased from Sigma-Aldrich Australia (Castle Hill, NSW, Australia), Sigma-Aldrich USA (St Louis, MO, USA), or Merck Chemicals (Kilsyth, Victoria, Australia) with the exception of isopropyl-β-D-thiogalactopyranoside (IPTG) and streptomycin (Life Technologies, Victoria, Australia), tetrodotoxin (Alomone Labs, Israel), and HPLC-grade acetonitrile (RCI Labscan, Bangkok, Thailand). $^{13}C_6$-glucose and $^{15}NH_4Cl$ were from Sigma-Aldrich Australia. Recombinant His_6-TEV protease (EC 3.4.22.44) was produced in-house using a published protocol[62].

Production of recombinant rDc1a

A synthetic gene encoding Dc1a, with codons optimised for expression in *Escherichia coli*, was produced and cloned into a variant of the pLIC-MBP expression vector by GeneArt (Invitrogen, Regensburg, Germany). This vector (pLIC-NSB3) encodes a MalE signal sequence for periplasmic export, a His_6 tag for affinity purification, a maltose binding protein (MBP) fusion tag to aid solubility, and a tobacco etch virus (TEV) protease recognition site directly preceding the codon-optimised Dc1a gene[23]. The plasmid encoding Dc1a was transformed into *E. coli* strain BL21(λDE3) for recombinant toxin production. Protein expression and purification were performed as described previously[30] with minor modifications. In summary, cultures were grown in Luria-Bertani broth at 37°C with shaking. Toxin gene expression was induced with 500 μM IPTG at an OD_{600} of 1.0–1.1, then cells were grown at 20 °C for a further 12 h before harvesting by centrifugation for 15 min at 10,500x*g* For production of uniformly $^{13}C/^{15}N$-labelled rDc1a, cultures were grown in minimal medium supplemented with $^{13}C_6$-glucose and $^{15}NH_4Cl$ as the sole carbon and nitrogen sources respectively. The His_6-MBP-toxin fusion protein was extracted from the bacterial periplasm by cell disruption at 27 kPa (TS Series Cell Disrupter, Constant Systems Ltd, Northants, UK), and then captured by passing the extract (buffered in 40 mM Tris, 450 mM NaCl, pH 8.0) over Ni-NTA Superflow resin (Qiagen, Chadstone, Australia). Proteins bound non-specifically were removed by washing with 10 mM imidazole then the fusion protein was eluted with 600 mM imidazole. The eluted fusion protein was concentrated to 10 ml and the buffer was exchanged to remove imidazole. Reduced and oxidised glutathione were then added to a final concentration of 0.6 mM and 0.4 mM, respectively, to maintain TEV protease activity and promote folding of the protein. Approximately 100 μg of His_6-tagged TEV protease was added per mg of rDc1a, then the cleavage reaction was allowed to proceed at room temperature for 12 h. The cleaved His_6-MBP and His_6-TEV were precipitated by addition of 1% trifluoroacetic acid (TFA), then the sample was centrifuged at 16,000x*g*. The supernatant was filtered using a 0.45 μm syringe filter (Millipore, MA, USA) and subjected to further purification using RP-HPLC. RP-HPLC was performed on a Vydac C18 column (250 × 4.6 mm, particle size 5 μm) using a flow rate of 1 ml/min and a gradient of 20–45% Solvent B (0.043% trifluoroacetic acid (TFA) in 90% acetonitrile) in Solvent A (0.05% TFA in water) over 30 min. rDc1a contains a non-native N-terminal serine residue (a vestige of the TEV protease cleavage site), making it one-residue longer than native Dc1a.

Mass spectrometry

Toxin masses were confirmed by matrix-assisted laser desorption/ionization time-of-flight mass spectrometry (MALDI-TOF MS) using a Model 4700 Proteomics Bioanalyser (Applied Biosystems, CA, USA). RP-HPLC fractions were mixed (1:1 v:v) with α-cyano-4 hydroxycinnamic acid matrix (5 mg/ml in 50/50 acetonitrile/H_2O) and MALDI-TOF spectra were acquired in positive reflector mode. All reported masses are for monoisotopic $[M + H]^+$ ions.

Structure determination

Several buffer conditions were screened to optimize quality of NMR data recorded for rDc1a, including 20 mM phosphate buffer, pH 6.0; 20 mM MES buffer, pH 6.0 and 20 mM acetate buffer pH 5.0. Initial buffer screening revealed the acetate buffer, pH 5.0 was optimal for acquisition of NMR data. Recombinant $^{15}N/^{13}C$-labelled rDc1a was dissolved in 20 mM acetate buffer, pH 5.0 to a final concentration of 350 μM. 5% ^2H_2O was added, then the sample was filtered using a low-protein-binding Ultrafree-MC centrifugal filter (0.22 μm pore size; Millipore, MA, USA) and 300 μL was added to a susceptibility matched 5 mm outer-diameter microtube (Shigemi Inc., Japan). NMR data were acquired at 25°C using a 900 MHz NMR spectrometer (Bruker BioSpin, Germany) equipped with a cryogenically cooled probe. 3D and 4D data used for resonance assignments were acquired using non-uniform sampling (NUS). Sampling schedules that approximated the signal decay in each indirect dimension were generated using sched3D[26]. NUS data were processed using the Rowland NMR toolkit (www.rowland.org/rnmrtk/toolkit.html) and maximum entropy parameters were automatically selected as previously described[63]. ^{13}C- and ^{15}N-edited HSQC-NOESY (mixing time of 200 ms) experiments were acquired using uniform sampling. All experiments were acquired in H_2O containing 5% ^2H_2O. Dihedral angles (ϕ, ψ) were derived from TALOS+ chemical shift analysis[64] and the restraint range for structure calculations was set to twice the estimated standard deviation. The Gly9–Pro10 and Arg36–Pro37 peptide bond was determined to be in the *trans* conformation on the basis of characteristic NOEs and the C_α and C_β chemical shifts of Pro residues. NOESY spectra were manually peak picked and integrated, then peak lists were automatically assigned, distance restraints extracted, and an ensemble of structures calculated using the torsion angle dynamics package CYANA 3.0[25]. The tolerances used for CYANA 3.0 were 0.025 ppm in the direct ^1H dimension, 0.03 ppm in the indirect ^1H dimension, and 0.3 ppm for the heteronucleus ($^{13}C/^{15}N$). During the automated NOESY assignment/structure calculation process, CYANA assigned 92% of all NOESY crosspeaks (2271 out of 2469).

Insecticidal assays

rDc1a was dissolved in insect saline and injected into the ventro-lateral thoracic region of adult sheep blowflies (*Lucilia cuprina*;), adult houseflies (*M. domestica*), adult American cockroaches (*Periplaneta americana*) and adult German cockroaches (*Blatella germanica*)[65]. Injections were made using a 1.0 ml Terumo Insulin syringe (B-D Ultra-Fine, Terumo Medical Corporation, Maryland, USA) with a fixed 29 G needle fitted to an Arnold hand micro-applicator (Burkard Manufacturing Co. Ltd., England). A maximum volume of 2 μl was injected per *L. cuprina*, *M. domestica* and *B. germanica* and 5 μl for the larger *P.*

americana. Thereafter, flies were individually housed in 2-ml tubes and provided with 10% sucrose while cockroaches were housed in closed Petri dishes and provided with dry food and water. The paralytic activity was then determined over a 24 h period. For each acute toxicity assay up to fourteen doses of rDc1a (n = 10 insects per dose) and the appropriate control (insect saline; n = 10 insects) were used. The assay was repeated three times. Median knockdown (KD_{50}) and median lethal (LD_{50}) doses were calculated as described previously[66] and averaged to produce KD_{50} and LD_{50} values.

Electrophysiological measurements on DUM neurons

DUM neurons were isolated from unsexed adult American cockroaches (*P. americana*) as described previously[30]. Briefly, terminal abdominal ganglia were removed and placed in normal insect saline (NIS) containing (in mM): NaCl 180, KCl 3.1, *N*-hydroxyethylpiperazine-*N*-ethanesulfonic acid (HEPES) 10 and D-glucose 20. Ganglia were then incubated in 1 mg/ml collagenase (type IA) for 40 min at 29°C. Following enzymatic treatment, ganglia were washed three times in NIS and triturated through a fire-polished Pasteur pipette. The resultant cell suspension was then distributed onto 12-mm diameter glass coverslips pre-coated with 2 mg/ml concanavalin A (type IV). DUM neurons were maintained in NIS supplemented with 5 mM $CaCl_2$, 4 mM $MgCl_2$, 5% foetal bovine serum and 1% penicillin and streptomycin (Life Technologies, Victoria, Australia), and maintained at 29 °C, 100 % humidity. Ionic currents were recorded in voltage-clamp mode using the whole-cell patch-clamp technique employing version 10.2 of the pCLAMP data acquisition system (Molecular Devices, Sunnyvale, CA). Data were filtered at 5–10 kHz with a low-pass Bessel filter with leakage and capacitive currents subtracted using $-P/4$ procedures. Digital sampling rates were set between 15 and 25 kHz depending on the length of the protocol. Single-use 0.8–2.5 MΩ electrodes were pulled from borosilicate glass and fire-polished prior to current recordings. Liquid junction potentials were calculated using JPCALC, and all data were compensated for these values. Cells were bathed in external solution through a continuous pressurized perfusion system at 1 ml/min, while toxin solutions were introduced via direct pressurized application via a perfusion needle at ~50 µl/min (Automate Scientific, San Francisco, CA). Control data were not acquired until at least 20 min after whole-cell configuration was achieved to eliminate the influence of fast time-dependent shifts in steady-state inactivation resulting in Na_V channel current (I_{Na}) rundown. All experiments were performed at ambient room temperature (20–23°C). To record I_{Na}, the external bath solution contained (in mM): NaCl 80, CsCl 5, $CaCl_2$ 1.8, tetraethylammonium chloride 50, 4-aminopyridine 5, HEPES 10, $NiCl_2$ 0.1, and $CdCl_2$ 1, adjusted to pH 7.4 with 1 M NaOH. The pipette solution contained (in mM): NaCl 34, CsF 135, $MgCl_2$ 1, HEPES 10, ethylene glycol-bis(2-aminoethylether)-*N*,*N*,*N*′,*N*′-tetraacetic acid 5, and ATP-Na_2 3, adjusted to pH 7.4 with 1 M CsOH. To eliminate any influence of differences in osmotic pressure, all internal and external solutions were adjusted with sucrose to 400 ± 5 mOsmol/l. Experiments were rejected if there were large leak currents or currents showed signs of poor space clamping.

Off-line data analysis was performed using Axograph X version 1.3 or Clampfit 10 (Molecular Devices, USA). Voltage-activation relationships were obtained by measuring steady-state currents elicited by stepwise depolarizations of 5–10 mV from a holding

potential of −90 mV and calculating peak conductance (G_{Na}) using the following equation: $G=I_{Na}/(V_m-E_{rev})$ where G is peak conductance, I_{Na} is peak inward sodium current, V_m is the test potential, and E_{rev} is the reversal potential. Reversal potentials were individually estimated for each data set[67] by fitting the I_{Na}-V data with the following equation: $I_{Na}=[1+\exp(-0.03937 \times z \times (V_m-V_{1/2}))]^{-1} \times g \times (V_m-V_{rev})$ where z is the apparent gating charge, g is a factor related to the number of channels contributing to the macroscopic whole-cell I_{Na}, V_m is equal to the voltage potential of the pulse, and $V_{1/2}$ is the voltage at half-maximal activation. The normalized conductance was fitted to a two-state Boltzmann function of the form: $G/G_{max} = 1/(1+\exp((-0.3937 \times z \times (V_m-V_{1/2})))$ where G, z, V_m and $V_{1/2}$ have the same meaning. The voltage dependence of steady-state Na_v channel inactivation (h_∞/V) data were normalized to the maximum peak current in the control or maximum peak current and fitted using the following Boltzmann equation: $h_\infty=A/(1+\exp((V_m-V_{12})/k))$ where A is the fraction of control maximal peak I_{Na} (value of 1.0 under control conditions), $V_{1/2}$ is the midpoint of steady-state inactivation, k is the slope factor, and V_m is the prepulse voltage. The rate of recovery from fast inactivation data were fitted to the following single exponential function: $I/I_{max} = 1-\exp(-\tau/t)$ where τ is the time constant of current recovery. Dose–response curves to determine LD_{50} and KD_{50} values were fitted using the following form of the logistic equation: $y=1/(1+[x]/Dose_{50})^{nH}$ where x is the toxin dose, n_H the Hill coefficient (slope parameter), and $Dose_{50}$ is the median inhibitory dose causing lethality (LD_{50}) or knockdown (KD_{50}). Non-linear curve-fitting of data were performed using GraphPad Prism version 6.00c for Macintosh (GraphPad Software, San Diego) or Origin 8 (OriginLab, MA, USA). Comparisons of two sample means were made using a paired Student's t-test and differences were considered to be significant if $p < 0.05$. All data are presented as mean ± standard error of the mean (SEM) of n independent experiments.

Electrophysiological measurements on oocytes

Chimeras and channel mutants were generated using sequential polymerase chain reactions (PCRs) with $K_v2.1\Delta7$[68] and $BgNa_v1$[21] as templates. The Kv2.1Δ7 construct contains seven point mutations in the outer vestibule, rendering the channel sensitive to agitoxin-2. The DNA sequence of all constructs and mutants was confirmed by automated DNA sequencing and cRNA was synthesized using T7 polymerase (mMessage mMachine kit, Life Technologies, USA) after linearizing the DNA with appropriate restriction enzymes. Channel constructs including $hNa_v1.1$–$hNa_v1.7$ and hERG were expressed in *Xenopus* oocytes by themselves or, in the case of $BgNa_v1$, together with the TipE subunit[69] (1:5 molar ratio), and studied following 1–2 days incubation after cRNA injection (incubated at 17°C in 96mM NaCl, 2mM KCl, 5mM HEPES, 1mM $MgCl_2$ and 1.8mM $CaCl_2$, 50μg/ml gentamycin, pH 7.6 with NaOH) using two-electrode voltage-clamp recording techniques (OC-725C, Warner Instruments, USA) with a 150-μl recording chamber. Data were filtered at 4 kHz and digitized at 20 kHz using pClamp software (Molecular Devices, USA). Microelectrode resistances were 0.5–1 MΩ when filled with 3M KCl. For most K_v channel experiments, the external recording solution contained (in mM): 50 KCl, 50 NaCl, 5 HEPES, 1 $MgCl_2$, 0.3 $CaCl_2$, pH 7.6 with NaOH. For Na_v channel experiments, the external recording solution contained (in mM): 96 NaCl, 2 KCl, 5 HEPES, 1 $MgCl_2$ and 1.8 $CaCl_2$, pH 7.6 with NaOH. All experiments were performed at room temperature (~22 °C). Leak

and background conductances, identified by blocking the channel with agitoxin-2 (Alomone labs) or tetrodotoxin (TTX), were subtracted for most of the K_v or $BgNa_v1$ currents shown.

Voltage–activation relationships were obtained by measuring tail currents for K_v channels or steady-state currents and calculating conductance for Na_v channels. Protocols for other measurements are described in the figure legends. After addition of the toxin to the recording chamber, the equilibration between the toxin and the channel was monitored using weak depolarizations elicited at 5-s intervals. For all channels, we recorded voltage–activation relationships in the absence and presence of toxin. Off-line data analysis was performed using Clampfit 10 (Molecular Devices, USA), Origin 8.0 (Originlab) and Microsoft Solver (Microsoft Excel).

Supplementary Material

Refer to Web version on PubMed Central for supplementary material.

Acknowledgments

We would like to thank Ke Dong (Michigan State University), Kenton J Swartz (NIH), Peter Ruben (Simon Fraser University), Chris Ahern (University of Iowa), James Barrow (Johns Hopkins University/Lieber Institute for Brain Development), and Marie-France Martin-Eauclaire and Pierre E Bougis (University of Marseille) for sharing $BgNa_V1$/TipE, $K_V2.1$, $hNa_V1.4$, $hNa_V1.5$, hERG, and BomIV, respectively. We thank Sandipan Chowdhury and Carlos Villalba-Galea for helpful discussions and Geoff Brown (Department of Agriculture, Fisheries and Forestry, Brisbane) for supply of blowflies. Parts of the research in this publication were supported by the Australian Research Council (Discovery Grant DP130103813 to GFK) and the National Institute of Neurological Disorders and Stroke (NINDS) of the National Institutes of Health (NIH) under award number R00NS073797 (FB).

References

1. King GF, Escoubas P, Nicholson GM. Peptide toxins that selectively target insect Na_V and Ca_V channels. Channels. 2008; 2:100–116. [PubMed: 18849658]
2. Hille, B. Ion channels of excitable membranes. 3. Sinauer Associates, Inc; 2001.
3. Bosmans F, Martin-Eauclaire MF, Swartz KJ. Deconstructing voltage sensor function and pharmacology in sodium channels. Nature. 2008; 456:202–208. [PubMed: 19005548]
4. Bosmans F, Puopolo M, Martin-Eauclaire MF, Bean BP, Swartz KJ. Functional properties and toxin pharmacology of a dorsal root ganglion sodium channel viewed through its voltage sensors. J Gen Physiol. 2011; 138:59–72. [PubMed: 21670206]
5. Payandeh J, Scheuer T, Zheng N, Catterall WA. The crystal structure of a voltage-gated sodium channel. Nature. 2011; 475:353–358. [PubMed: 21743477]
6. Zhang X, et al. Crystal structure of an orthologue of the NaChBac voltage-gated sodium channel. Nature. 2012; 486:130–134. [PubMed: 22678295]
7. Milescu M, Bosmans F, Lee S, Alabi AA, Kim JI, Swartz KJ. Interactions between lipids and voltage sensor paddles detected with tarantula toxins. Nat Struct Mol Biol. 2009; 16:1080–1085. [PubMed: 19783984]
8. Dong K. Insect sodium channels and insecticide resistance. Invert Neurosci. 2007; 7:17–30. [PubMed: 17206406]
9. Soderlund DM. Molecular mechanisms of pyrethroid insecticide neurotoxicity: recent advances. Arch Toxicol. 2012; 86:165–181. [PubMed: 21710279]
10. Tan J, Soderlund DM. Divergent actions of the pyrethroid insecticides S-bioallethrin, tefluthrin, and deltamethrin on rat $Na_V1.6$ sodium channels. Toxicol Appl Pharmacol. 2010; 247:229–237. [PubMed: 20624410]
11. Zakon HH. Adaptive evolution of voltage-gated sodium channels: the first 800 million years. Proc Natl Acad Sci U S A. 2012; 109:10619–10625. [PubMed: 22723361]

12. Bosmans F, Swartz KJ. Targeting voltage sensors in sodium channels with spider toxins. Trends Pharmacol Sci. 2010; 31:175–182. [PubMed: 20097434]
13. Fry BG, et al. The toxicogenomic multiverse: convergent recruitment of proteins into animal venoms. Annual review of genomics and human genetics. 2009; 10:483–511.
14. Klint JK, et al. Spider-venom peptides that target voltage-gated sodium channels: pharmacological tools and potential therapeutic leads. Toxicon. 2012; 60:478–491. [PubMed: 22543187]
15. King GF, Hardy MC. Spider-venom peptides: structure, pharmacology, and potential for control of insect pests. Annual review of entomology. 2013; 58:475–496.
16. Boulton AM, Polis GA. Phenology and life history of the desert spider, *Diguetia majavea*. J Arachnol. 1999; 27:513–521.
17. Gertsch, WJ. The spider family Diguetidae. New York, NY: American Museum of Natural History; 1985. p. 1904
18. King GF, Gentz MC, Escoubas P, Nicholson GM. A rational nomenclature for naming peptide toxins from spiders and other venomous animals. Toxicon. 2008; 52:264–276. [PubMed: 18619481]
19. Krapcho KJ, Kral RM Jr, Vanwagenen BC, Eppler KG, Morgan TK. Characterization and cloning of insecticidal peptides from the primitive weaving spider *Diguetia canities*. Insect Biochem Mol Biol. 1995; 25:991–1000. [PubMed: 8541888]
20. Bloomquist JR, Kinne LP, Deutsch V, Simpson SF. Mode of action of an insecticidal peptide toxin from the venom of a weaving spider (*Diguetia canities*). Toxicon. 1996; 34:1072–1075. [PubMed: 8896202]
21. Dong K. A single amino acid change in the para sodium channel protein is associated with knockdown-resistance (kdr) to pyrethroid insecticides in German cockroach. Insect Biochem Mol Biol. 1997; 27:93–100. [PubMed: 9066120]
22. Moignot B, Lemaire C, Quinchard S, Lapied B, Legros C. The discovery of a novel sodium channel in the cockroach *Periplaneta americana*: evidence for an early duplication of the *para*-like gene. Insect Biochem Mol Biol. 2009; 39:814–823. [PubMed: 19800971]
23. Klint JK, et al. Production of recombinant disulfide-rich venom peptides for structural and functional analysis via expression in the periplasm of *E. coli*. PLoS One. 2013; 8:e63865. [PubMed: 23667680]
24. Mobli M, King GF. NMR methods for determining disulfide-bond connectivities. Toxicon. 2010; 56:849–854. [PubMed: 20603141]
25. Güntert P. Automated NMR structure calculation with CYANA. Methods Mol Biol. 2004; 278:353–378. [PubMed: 15318003]
26. Mobli M, Stern AS, Bermel W, King GF, Hoch JC. A non-uniformly sampled 4D HCC(CO)NH-TOCSY experiment processed using maximum entropy for rapid protein sidechain assignment. J Magn Reson. 2010; 204:160–164. [PubMed: 20299257]
27. Davis IW, et al. MolProbity: all-atom contacts and structure validation for proteins and nucleic acids. Nucleic Acids Res. 2007; 35:W375–W383. [PubMed: 17452350]
28. Kwan AH, Mobli M, Gooley PR, King GF, Mackay JP. Macromolecular NMR spectroscopy for the non-spectroscopist. Febs J. 2011; 278:687–703. [PubMed: 21214860]
29. Holm L, Rosenstrom P. Dali server: conservation mapping in 3D. Nucleic Acids Res. 2010; 38:W545–W549. [PubMed: 20457744]
30. Bende NS, et al. The insecticidal neurotoxin Aps III is an atypical knottin peptide that potently blocks insect voltage-gated sodium channels. Biochem Pharmacol. 2013; 85:1542–1554. [PubMed: 23473802]
31. Milescu M, et al. Tarantula toxins interact with voltage sensors within lipid membranes. J Gen Physiol. 2007; 130:497–511. [PubMed: 17938232]
32. Eberhard W. Attack behavior of diguetid spiders and the origin of prey wrapping in spiders. Psyche Cambridge. 1967; 74:173–181.
33. Liu Z, Song W, Dong K. Persistent tetrodotoxin-sensitive sodium current resulting from U-to-C RNA editing of an insect sodium channel. Proc Natl Acad Sci U S A. 2004; 101:11862–11867. [PubMed: 15280550]

34. Trudeau MC, Warmke JW, Ganetzky B, Robertson GA. HERG, a human inward rectifier in the voltage-gated potassium channel family. Science. 1995; 269:92–95. [PubMed: 7604285]
35. Cestele S, Yarov-Yarovoy V, Qu Y, Sampieri F, Scheuer T, Catterall WA. Structure and function of the voltage sensor of sodium channels probed by a beta-scorpion toxin. J Biol Chem. 2006; 281:21332–21344. [PubMed: 16679310]
36. Cestele S, Qu Y, Rogers JC, Rochat H, Scheuer T, Catterall WA. Voltage sensor-trapping: enhanced activation of sodium channels by β-scorpion toxin bound to the S3–S4 loop in domain II. Neuron. 1998; 21:919–931. [PubMed: 9808476]
37. Swartz KJ. Tarantula toxins interacting with voltage sensors in potassium channels. Toxicon. 2007; 49:213–230. [PubMed: 17097703]
38. Alabi AA, Bahamonde MI, Jung HJ, Kim JI, Swartz KJ. Portability of paddle motif function and pharmacology in voltage sensors. Nature. 2007; 450:370–375. [PubMed: 18004375]
39. Long SB, Tao X, Campbell EB, MacKinnon R. Atomic structure of a voltage-dependent K^+ channel in a lipid membrane-like environment. Nature. 2007; 450:376–382. [PubMed: 18004376]
40. Aggarwal SK, MacKinnon R. Contribution of the S4 segment to gating charge in the Shaker K^+ channel. Neuron. 1996; 16:1169–1177. [PubMed: 8663993]
41. Seoh SA, Sigg D, Papazian DM, Bezanilla F. Voltage-sensing residues in the S2 and S4 segments of the Shaker K^+ channel. Neuron. 1996; 16:1159–1167. [PubMed: 8663992]
42. Zagotta WN, Hoshi T, Aldrich RW. Shaker potassium channel gating. III: Evaluation of kinetic models for activation. J Gen Physiol. 1994; 103:321–362. [PubMed: 8189208]
43. Delemotte L, Tarek M, Klein ML, Amaral C, Treptow W. Intermediate states of the Kv1.2 voltage sensor from atomistic molecular dynamics simulations. Proc Natl Acad Sci U S A. 2011; 108:6109–6114. [PubMed: 21444776]
44. Jensen MO, Jogini V, Borhani DW, Leffler AE, Dror RO, Shaw DE. Mechanism of voltage gating in potassium channels. Science. 2012; 336:229–233. [PubMed: 22499946]
45. Tao X, Lee A, Limapichat W, Dougherty DA, MacKinnon R. A gating charge transfer center in voltage sensors. Science. 2010; 328:67–73. [PubMed: 20360102]
46. Gagnon DG, Bezanilla F. A single charged voltage sensor is capable of gating the Shaker K+ channel. J Gen Physiol. 2009; 133:467–483. [PubMed: 19398775]
47. Lacroix JJ, et al. Intermediate state trapping of a voltage sensor. J Gen Physiol. 2012; 140:635–652. [PubMed: 23183699]
48. Buraei Z, Anghelescu M, Elmslie KS. Slowed N-type calcium channel (CaV2.2) deactivation by the cyclin-dependent kinase inhibitor roscovitine. Biophys J. 2005; 89:1681–1691. [PubMed: 15951378]
49. Capes DL, Goldschen-Ohm MP, Arcisio-Miranda M, Bezanilla F, Chanda B. Domain IV voltage-sensor movement is both sufficient and rate limiting for fast inactivation in sodium channels. J Gen Physiol. 2013; 142:101–112. [PubMed: 23858005]
50. Chanda B, Bezanilla F. Tracking voltage-dependent conformational changes in skeletal muscle sodium channel during activation. J Gen Physiol. 2002; 120:629–645. [PubMed: 12407076]
51. Sheets MF, Kyle JW, Kallen RG, Hanck DA. The Na channel voltage sensor associated with inactivation is localized to the external charged residues of domain IV, S4. Biophys J. 1999; 77:747–757. [PubMed: 10423423]
52. Cestele S, et al. Scorpion α-like toxins, toxic to both mammals and insects, differentially interact with receptor site 3 on voltage-gated sodium channels in mammals and insects. Eur J Neurosci. 1999; 11:975–985. [PubMed: 10103091]
53. Tan J, Liu Z, Nomura Y, Goldin AL, Dong K. Alternative splicing of an insect sodium channel gene generates pharmacologically distinct sodium channels. J Neurosci. 2002; 22:5300–5309. [PubMed: 12097481]
54. Bourdin CM, et al. Intron retention in mRNA encoding ancillary subunit of insect voltage-gated sodium channel modulates channel expression, gating regulation and drug sensitivity. PLoS One. 2013; 8:e67290. [PubMed: 23967047]
55. Catterall WA, Cestele S, Yarov-Yarovoy V, Yu FH, Konoki K, Scheuer T. Voltage-gated ion channels and gating modifier toxins. Toxicon. 2007; 49:124–141. [PubMed: 17239913]

56. Xiao Y, Jackson JO 2nd, Liang S, Cummins TR. Common molecular determinants of tarantula huwentoxin-IV inhibition of Na_+ channel voltage sensors in domains II and IV. J Biol Chem. 2011; 286:27301–27310. [PubMed: 21659528]
57. Saez NJ, et al. Spider-venom peptides as therapeutics. Toxins. 2010; 2:2851–2871. [PubMed: 22069579]
58. Krepkiy D, et al. Structure and hydration of membranes embedded with voltage-sensing domains. Nature. 2009; 462:473–479. [PubMed: 19940918]
59. Zhang JZ, et al. Structure-function map of the receptor site for β-scorpion toxins in domain II of voltage-gated sodium channels. J Biol Chem. 2011; 286:33641–33651. [PubMed: 21795675]
60. Song W, et al. Substitutions in the domain III voltage-sensing module enhance the sensitivity of an insect sodium channel to a scorpion β-toxin. J Biol Chem. 2011; 286:15781–15788. [PubMed: 21454658]
61. Corzo G, et al. Distinct primary structures of the major peptide toxins from the venom of the spider *Macrothele gigas* that bind to sites 3 and 4 in the sodium channel. FEBS Lett. 2003; 547:43–50. [PubMed: 12860384]
62. Fang L, Jia KZ, Tang YL, Ma DY, Yu M, Hua ZC. An improved strategy for high-level production of TEV protease in *Escherichia coli* and its purification and characterization. Protein Expr Purif. 2007; 51:102–109. [PubMed: 16919473]
63. Mobli M, Maciejewski MW, Gryk MR, Hoch JC. An automated tool for maximum entropy reconstruction of biomolecular NMR spectra. Nat Methods. 2007; 4:467–468. [PubMed: 17538627]
64. Shen Y, Delaglio F, Cornilescu G, Bax A. TALOS+: a hybrid method for predicting protein backbone torsion angles from NMR chemical shifts. J Biomol NMR. 2009; 44:213–223. [PubMed: 19548092]
65. Eitan M, Fowler E, Herrmann R, Duval A, Pelhate M, Zlotkin E. A scorpion venom neurotoxin paralytic to insects that affects sodium current inactivation: purification, primary structure, and mode of action. Biochemistry. 1990; 29:5941–5947. [PubMed: 2383565]
66. Herzig V, Hodgson WC. Neurotoxic and insecticidal properties of venom from the Australian theraphosid spider *Selenotholus foelschei*. Neurotoxicology. 2008; 29:471–475. [PubMed: 18423874]
67. Zhou W, Goldin AL. Use-dependent potentiation of the Nav1.6 sodium channel. Biophys J. 2004; 87:3862–3872. [PubMed: 15465873]
68. Swartz KJ, MacKinnon R. Hanatoxin modifies the gating of a voltage-dependent K^+ channel through multiple binding sites. Neuron. 1997; 18:665–673. [PubMed: 9136774]
69. Feng G, Deak P, Chopra M, Hall LM. Cloning and functional analysis of TipE, a novel membrane protein that enhances *Drosophila para* sodium channel function. Cell. 1995; 82:1001–1011. [PubMed: 7553842]
70. Nguyen MN, Tan KP, Madhusudhan MS. CLICK--topology-independent comparison of biomolecular 3D structures. Nucleic Acids Res. 2011; 39:W24–28. [PubMed: 21602266]

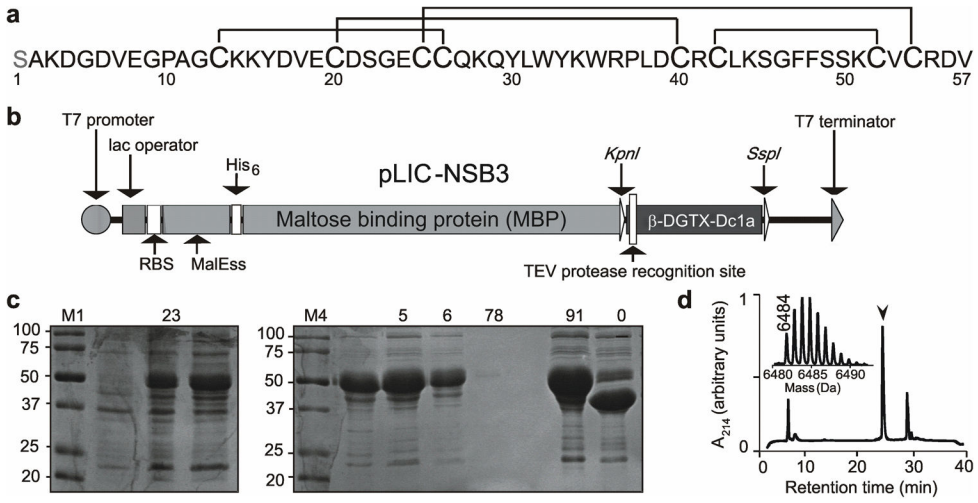

Figure 1. Recombinant production of Dc1a

a, Primary structure of rDc1a. The non-native N-terminal Ser residue that is a vestige of the TEV protease cleavage site used for recombinant toxin production is highlighted in grey. Disulfide bridge connectivity is shown above the sequence. **b,** Schematic representation of the pLicC-NSB3 vector used for periplasmic expression of rDc1a. The coding region includes a MalE signal sequence ($MalE_{SS}$) for periplasmic export, a His_6 affinity tag, an MBP fusion tag, and a codon-optimized gene encoding rDc1a, with a TEV protease recognition site inserted between the MBP and toxin coding regions. The locations of key elements of the vector are shown, including the ribosome-binding site (RBS). **c,** SDS-PAGE gels illustrating different steps in the purification of rDc1a. Lanes contain: M, molecular weight markers; lane 1, *E. coli* cell extract prior to IPTG induction; lane 2, *E. coli* cell extract after IPTG induction; lane 3, soluble periplasmic extract (the His_6-MBP-rDc1a fusion protein is evident at ~50 kDa); lane 4, Ni-NTA beads after loading the cell lysate; lane 5, eluate-1 from washing Ni-NTA resin with 600 mM imidazole; lane 6, elute-2 from washing Ni-NTA resin with 600 mM imidazole; lane 7, eluate-3 from washing Ni-NTA resin with 600 mM imidazole; lane 8, Ni-NTA beads after elution-3; lane 9, fusion protein sample before TEV protease cleavage; lane 10, fusion protein sample after TEV protease cleavage showing almost complete cleavage of fusion protein to His_6-MBP. **d,** RP-HPLC chromatogram showing the final step in the purification of rDc1a. The arrow denotes the peak corresponding to correctly folded recombinant rDc1a. Inset is a MALDI-TOF MS spectrum showing the $[M+H]^+$ ion for the purified recombinant toxin (obs. = 6484 Da; calc. = 6485.39 Da).

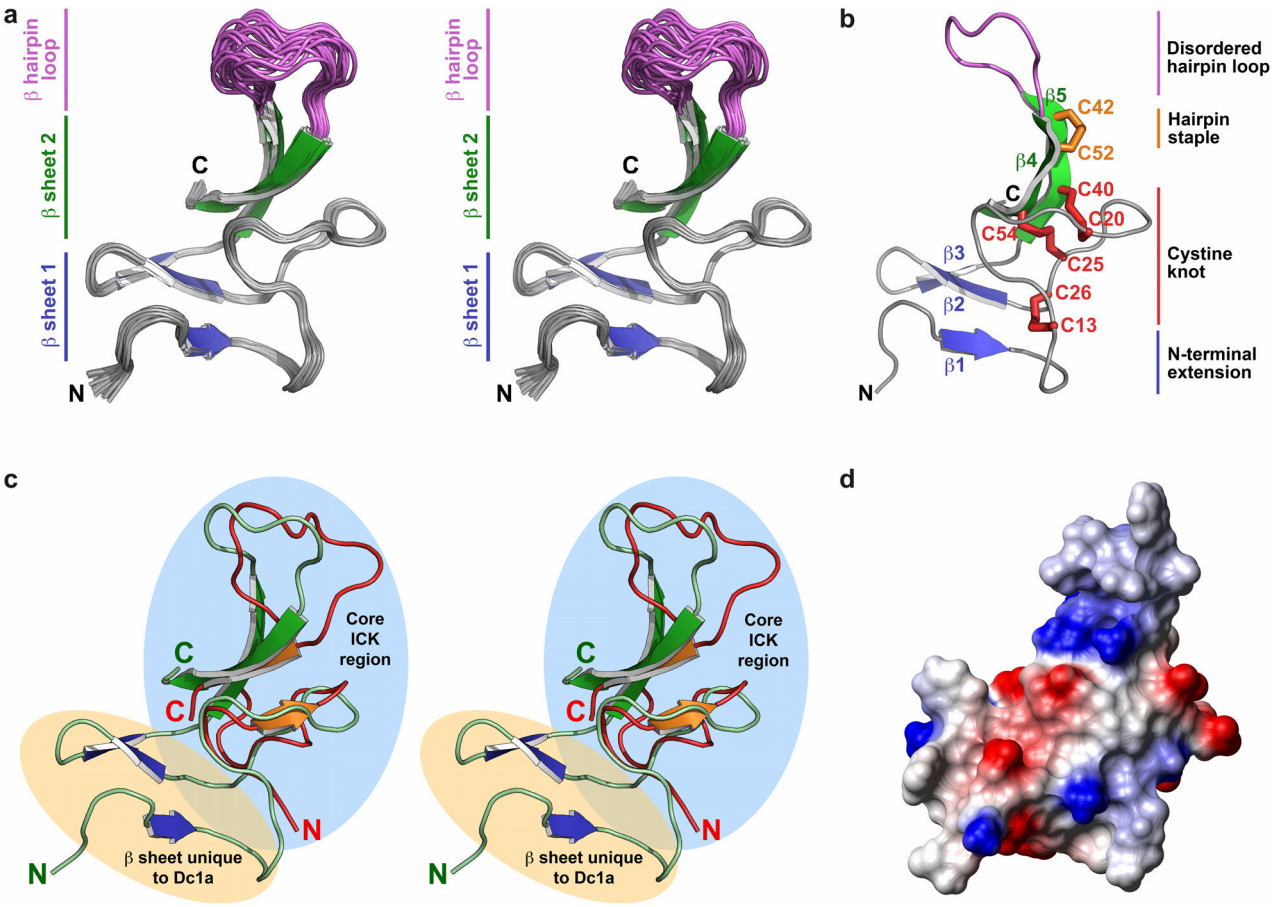

Figure 2. NMR solution structure of rDc1a

a, Stereo view of the ensemble of 20 rDc1a structures. The structures are overlaid over the backbone atoms of residues 2–42 and 52–56 in order to highlight the disordered nature of the hairpin loop (residues 43–51, purple) relative to the well-structured ICK region of the toxin. The N- and C-termini are labeled and the β-strands that form the N- and C-terminal β-sheets are colored blue and green, respectively. **b,** Ribbon representation of rDc1a highlighting the five βstrands (β1–β5) and four disulfide bonds. The three disulfide bonds that form the ICK motif are shown in red while the fourth disulfide that staples the base of the disordered β4–β5 hairpin loop is highlighted in orange. The β-strands and disordered hairpin loop are colored as in panel **a. c,** Stereo view of the structures of As1a, a typical knottin peptide[30], overlaid with rDc1a. The two structures were overlaid for optimal superposition over their core ICK regions (28 residues; region highlighted in cyan) using the CLICK server[70]. Note that the N-terminal β-sheet in rDc1a is quite distinct from the region of structural overlap. **d,** Electrostatic surface potential of rDc1a with positive and negative charges shown in blue and red, respectively. The molecular orientation is the same as in panels **a** and **c**.

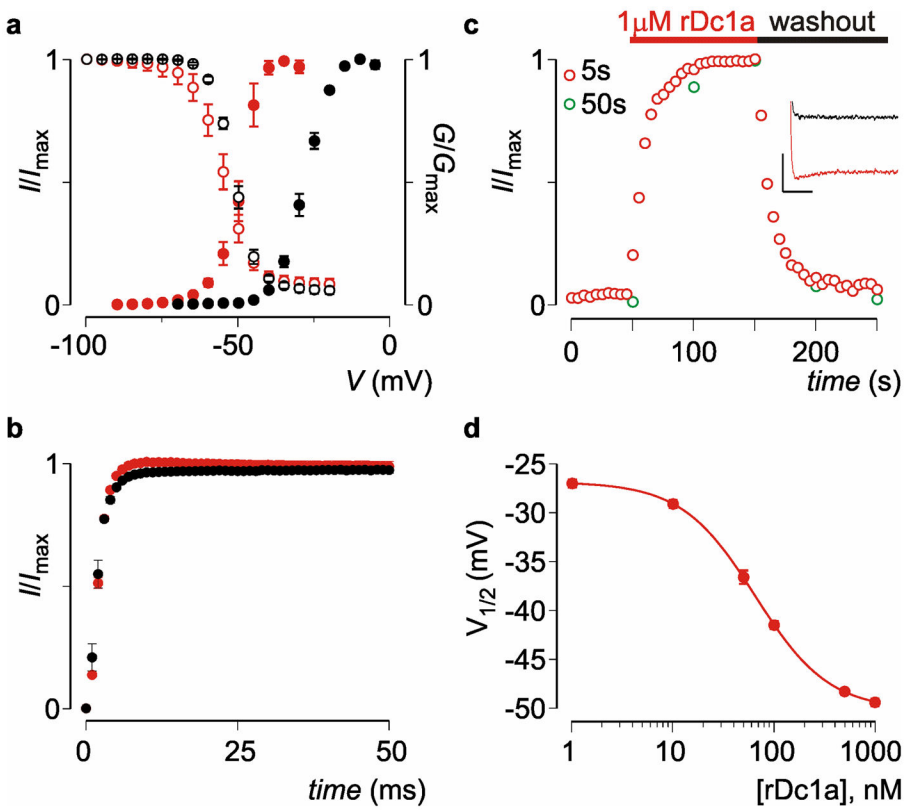

Figure 3. rDc1a promotes opening of BgNa$_v$1 channels

a, Comparison of the gating properties of BgNa$_v$1 before (black) and after (red) addition of 1 μM rDc1a. Shown are the normalized deduced conductance (*G*)–voltage (filled circles) (G/G_{max}) and steady-state inactivation (open circles; I/I_{max}) relationships. Currents were elicited by 5-mV step depolarizations from a holding voltage of −90 mV or −100 mV, respectively. n = 3–5, and error bars represent SEM. Descriptive values resulting from Boltzmann fits can be found in *Results* section. **b,** Recovery from fast inactivation of WT BgNa$_v$1 before (black) and after (red) addition of 1 μM rDc1a (red) determined by a double-pulse protocol to −30 mV with a varying time between pulses (0–50 ms). Values are reported in the *Results* section. Data represents n = 4 experiments, and error bars represent the SEM. **c,** Upon addition of 1 μM rDc1a to channels depolarized to −60 mV every 5 s (red open circles) or 50 s (green open circles) (holding voltage was −100 mV), BgNa$_v$1-mediated sodium currents become rapidly visible. Channels completely recover after toxin washout. Inset shows current trace before (black) and after (red) addition of 1 μM rDc1a at −60 mV (5 s pulses). Noticeable is the persistent current that appears at this voltage, even in control experiments. Abscissa scale is 10 ms, ordinate scale is 0.3 μA. **d,** Concentration dependence of rDc1a-induced current potentiation determined from shifts in the midpoint of channel activation ($V_{1/2}$). Line represents a fit of the data with the Hill equation resulting in a half maximal concentration (EC_{50}) of 65 ± 1 nM and a slope factor of 1.19 ± 0.02; n = 5 and error bars represent SEM.

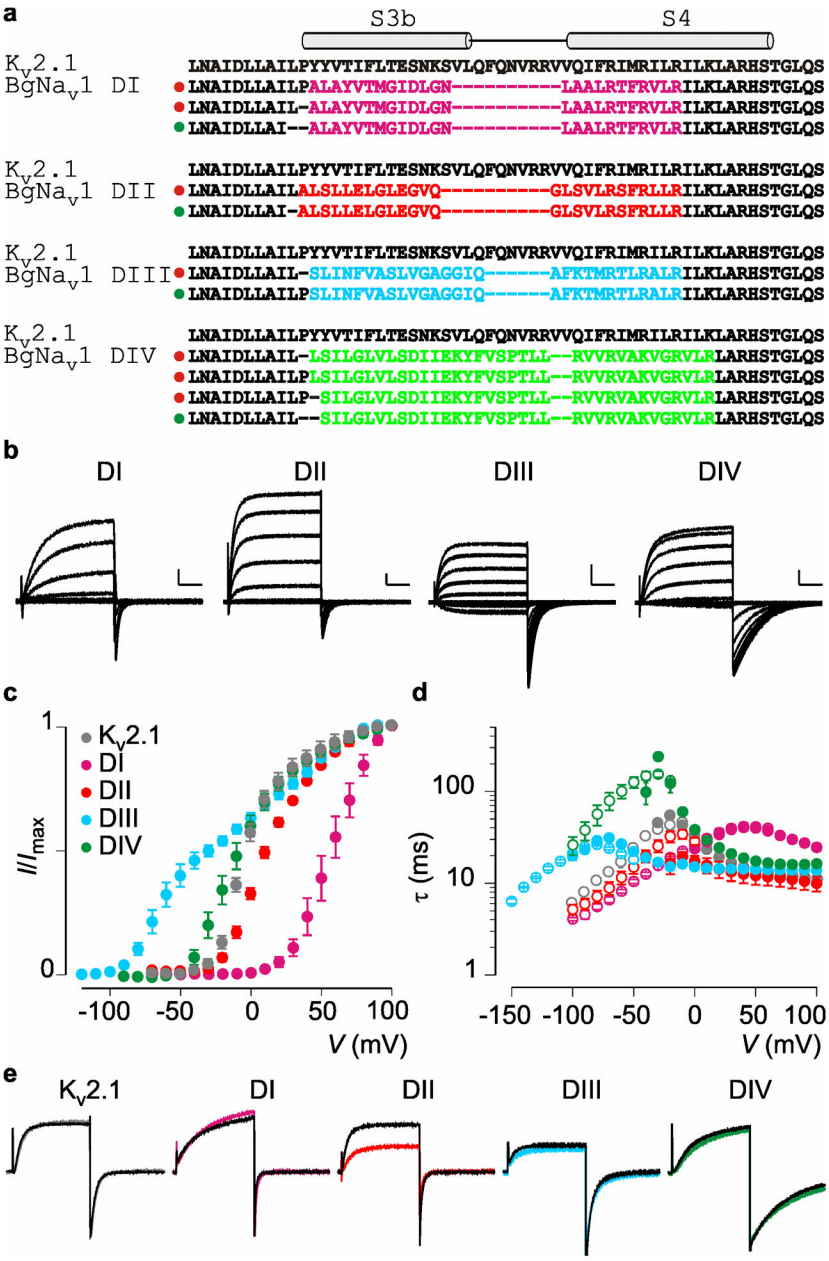

Figure 4. Transfer of the voltage sensor paddle motifs from $BgNa_v1$ to $K_v2.1$

a, Sequence alignment of the paddle region of $K_v2.1$ with the separate S3b–S4 regions of $BgNa_v1$ arranged per domain. In $BgNa_v1$, the paddle motifs are not identical and are therefore colored differently: purple, domain I paddle (DI); red, domain II paddle (DII); blue, domain III paddle (DIII); green, domain IV paddle (DIV). In $K_v2.1$, the paddle motifs are identical and therefore have the same color (black). Functional chimeras are indicated with a green dot in front of the sequence whereas non-functional chimeras are indicated with a red dot. **b,** and **c,** Transfer of the $BgNa_v1$ paddle motifs into $K_v2.1$. Families of potassium currents (**b**) and tail current voltage–activation relationships (**c**) for each chimeric construct (n = 6; error bars represent SEM). Holding voltage was −90 mV for DI, II, and IV, and −120

mV for DIII, and the tail voltage was −60 mV (−100 mV for DIII). Bars in **b** are 1 μA and 100 ms. **d,** Kinetics of opening and closing for $K_v2.1$ channels containing paddle motifs from the four domains of $BgNa_v1$. Mean time constants (τ) from single-exponential fits to channel activation (filled circles) and deactivation (open circles) are plotted as a function of the voltage at which the current was recorded. $n = 6$, and error bars represent SEM. **e,** Potassium currents elicited by depolarizations near the foot (less than 1/3 of maximal activation) of the voltage-activation curve (**c**) for $BgNa_v1/K_v2.1$ chimeric constructs. Currents are shown prior to (black) and following (colored) addition of 1 μM rDc1a. rDc1a clearly affects only the DII chimera.

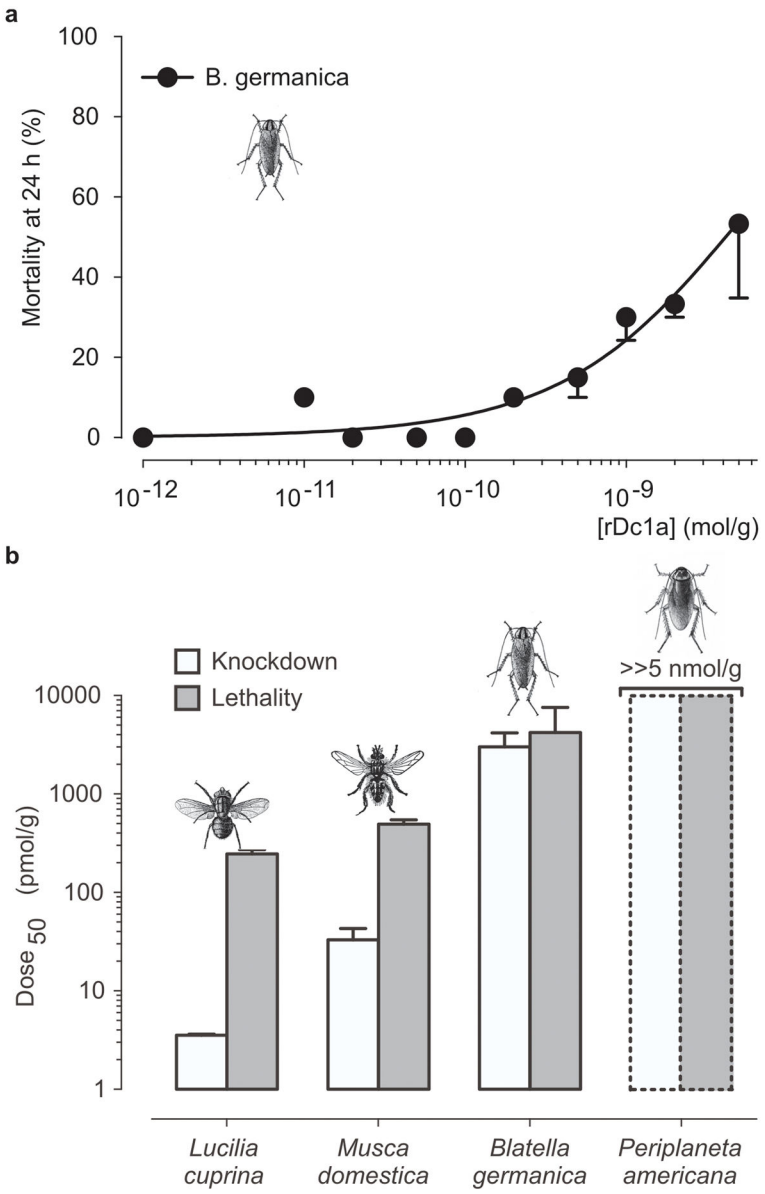

Figure 5. Acute toxicity of rDc1a in two cockroach families

a, Dose–response curve for lethal effects of rDc1a determined 24 h after injection into German cockroaches (*B. germanica*; family Blattellidae, closed circles). Data were fitted according to Eq. 5 in *Materials and Methods* and represent mean ± SEM of 3 independent experiments. **b,** Comparison of the KD_{50} (open columns) and LD_{50} (gray columns) doses at 24 h following injection of rDc1a in *L. cuprina*, *M. domestica*, and *B. germanica*. Note: Doses up to 5 nmol/g failed to produce any signs of knockdown or lethality up to 72 h post injection in American cockroaches (*Periplaneta americana*; family Blattellidae). Data represent mean ± SEM of 3 independent experiments

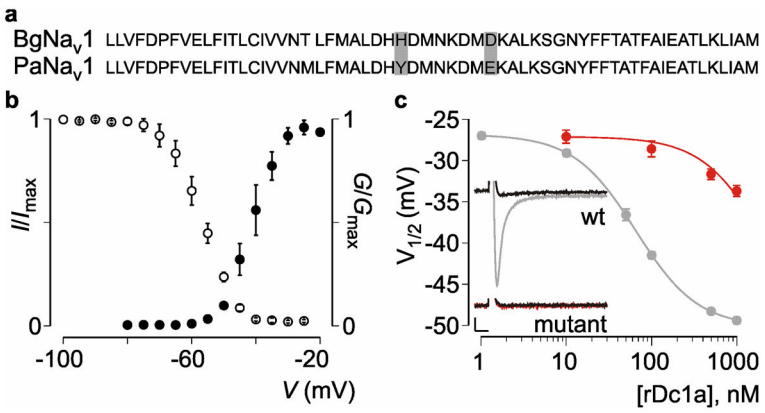

Figure 6. Residues outside of the DII paddle motif contribute to rDc1a binding

a, Sequence alignment of the DII S1-S2 regions of $BgNa_v1$ and $PaNa_v1$ (See Supplementary Fig. 4 for more details). In the extracellular loop connecting S1 to S2, all residues are identical except the H805Y and D812E substitutions (gray background). The T797M substitution within S1 is unlikely to be toxin-accessible. **b,** Gating properties of the mutant $BgNa_v1^{YE}$ channel. Shown are the normalized deduced conductance (*G*)–voltage (filled circles) (G/G_{max}) and steady-state inactivation (open circles; I/I_{max}) relationships. Descriptive values can be found in *Results* section. Currents were elicited by 5 mV step depolarizations from a holding voltage of −90 mV or −100 mV, respectively. n = 3–5, and error bars represent SEM. **c,** Affinity measure for rDc1a interaction with $BgNa_v1^{YE}$ (red) compared to WT $BgNa_v1$ (gray). Concentration dependence for toxin-induced current potentiation (as determined by shifts in $V_{1/2}$) is shown. It is clear that alterations in channel opening upon rDc1a exposure are less pronounced with the $BgNa_v1^{YE}$ mutant when compared to WT $BgNa_v1$. n = 5 and error bars represent SEM. Inset shows premature channel opening after addition of 100 nM rDc1a to WT $BgNa_v1$ (grey) whereas $BgNa_v1^{YE}$ is not yet affected (red). Current traces were evoked by a 50 ms depolarization to −55 mV from a holding potential of −90 mV.